High-resolution electron energy loss spectra of reconstructed Si(100) surfaces: First-principles study

Lucia Caramella,[1] Conor Hogan,[2] Giovanni Onida,[1] and Rodolfo Del Sole[2]
[1]*Dipartimento di Fisica, European Theoretical Spectroscopy Facility (ETSF), Università degli Studi di Milano, via Celoria 16, 20133 Milano, Italy*
[2]*Dipartimento di Fisica, European Theoretical Spectroscopy Facility (ETSF), and CNR-INFM-SMC, Università di Roma "Tor Vergata," Via della Ricerca Scientifica 1, 00133 Roma, Italy*
(Received 24 January 2009; revised manuscript received 27 March 2009; published 28 April 2009)

We present *ab initio* calculations of electron energy loss spectroscopy in the reflection geometry (REELS) for the Si(100) surface for which several experimental data are available. The standard surface models [$p(2\times1)$, $c(4\times2)$, and $p(2\times2)$] are structurally very similar in nature, and precise calculations are necessary to differentiate between them. Starting from optimized geometries we compute REELS spectra within the framework of the three-layer model. We adopt several methodologies to ensure a realistic model of the experiment, including a precise partitioning of the surface and bulk dielectric functions and a numerical integration over the detector aperture. We obtain good agreement with the various available experimental energy loss and reflectance anisotropy spectra. The calculations allow us to definitively rule out the presence of the $p(2\times1)$ reconstruction. We interpret the S_0 peak observed by Farrell *et al.* [Phys. Rev. B **30**, 721 (1984)] in high resolution REELS. Furthermore, we explain the observed dependence of the spectra on temperature by inferring the presence of dimer flipping at room temperature.

DOI: 10.1103/PhysRevB.79.155447 PACS number(s): 78.68.+m, 73.20.At, 31.15.A−

I. INTRODUCTION

Due to its enormous technological importance, the Si(100) surface has been the subject of a wide range of experimental and theoretical studies spanning several decades. In fact, high impact publications continue to appear regarding the atomic structure and electronic properties of even the clean surface. Following early low-energy electron diffraction (LEED) experiments,[1] it was understood that Si(100) forms a $p(2\times1)$ reconstruction. The classic explanation of the LEED observation is that the surface is composed of rows of Si dimers separated by trenches, as confirmed by various scanning tunneling microscopy (STM) studies.[2,3] Although some quantum chemistry studies have found that a symmetric dimer structure (causing a metallic surface) forms the global minimum,[4] several total energy calculations based on density-functional theory[5] have found that dimer buckling induces a small energy gain, such that the dimers adopt an asymmetric configuration and the surface remains semiconducting.[6]

Three distinct structures have been proposed for the Si(100) surface: the $p(2\times1)$, whereby all dimers are buckled the same way [Fig. 1(a)]; the $p(2\times2)$ structure, where alternating dimers in a row are buckled in opposite directions and adjacent rows are buckled in phase [Fig. 1(b)]; and the $c(4\times2)$ phase, being the same as the $p(2\times2)$ but with adjacent rows buckled out of phase [Fig. 1(c)]. Total energy calculations have found[5] that the $p(2\times1)$ reconstruction is prohibitively higher in energy than the other two (at 0 K) and that the $c(4\times2)$ is only slightly favored over the $p(2\times2)$.

Which reconstruction is formed on the surface depends critically on the temperature. LEED studies have shown that an order-disorder phase transition occurs at about 200 K.[7,8] Below this critical temperature, a $c(4\times2)$ phase is generally observed; above it, a $p(2\times1)$ periodicity is seen. Direct observation of the surface structure with STM is complicated by two factors however. First, it is now widely suggested that the experimental measurement itself can influence the result and drive $c(4\times2)\rightarrow p(2\times2)$ phase transitions.[9,10] Charge injection, or electric fields induced by the STM tip, can cause dimers to flip, according to various experimental[10,11] and theoretical works.[12,13] Nevertheless, the general consensus is that the $c(4\times2)$ reconstruction is the most stable structure below the critical temperature.[10,14]

Above 200 K, STM images appear to show a symmetric dimer configuration. However, at these temperatures the dimer rocking mode is activated, and hence it is believed that the observed symmetric $p(2\times1)$ structure is merely a time average of the thermal flip-flop motion of the buckled dimers. Based on molecular dynamics simulation of the dimer motion, it was suggested that the surface consists of a simultaneous local presence of asymmetric dimers and instantaneously flat symmetric dimers.[15] This work and more recent studies (see Refs. 32–35 in Ref. 16) have suggested that the dimers remain short-range correlated. In particular, a two-photon-photoemission study found minor difference between the surface band dispersion at 90 K and at room temperature.[17]

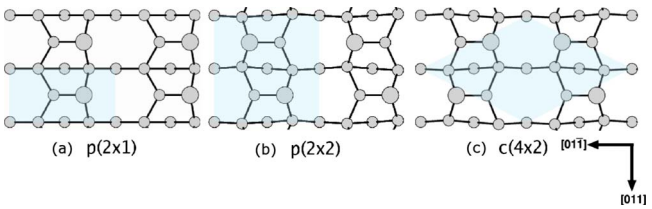

FIG. 1. (Color online) Ball and stick model of Si(100) $p(2\times1)$, $p(2\times2)$, and $c(4\times2)$ surface reconstructions. Large circles indicate "up" silicon dimer atoms. Unit cells are indicated by shaded regions.

Theoretical simulations of the reflectance anisotropy (RA) spectra confirm that the $p(2\times1)$ reconstruction does not reproduce correctly the experimental line shape.[18–20] On the other hand, both $c(4\times2)$ and $p(2\times2)$ structures are quite similar to the experiment, with the $c(4\times2)$ yielding a slightly better agreement. Simulation of the surface differential reflectance (SDR) also favors the $c(4\times2)$ surface,[18] in particular predicting the observed SDR structure below 1 eV.

In addition to optical techniques such as RA or SDR, electron energy loss spectroscopy (EELS) in the reflection geometry (REELS or RELS) offers an enhanced surface sensitivity and easy access to a wide energy range. Although the majority of literature considering REELS of Si(100) has focused on vibrational properties,[21] several studies have examined the nature of electronic states at the clean Si(100) surface.[22,23] However, the resolution available in these works was not high enough to yield precise spectra, and hence second-derivative spectra were reported. Indirect information about surface states was derived from related studies looking at the changes in the REELS spectrum following oxidation.[24–26] High-resolution electron energy loss spectroscopy (HREELS) measurements were later carried out by Farrell *et al.*[27] and Gavioli *et al.*[28] In the latter work, tight binding calculations were also performed on the $p(2\times1)$ symmetric and asymmetric dimer models, and it was suggested that a mixture of the two structures was necessary to explain the room temperature EELS spectra. However, the $c(4\times2)$ structure was not considered in that work, and therefore some of the conclusions reached cannot be complete.

In this work, we present a thorough computational study of high-resolution EELS for the different reconstructions of clean Si(100), taking into account various technicalities that arise in the simulation of the experiment. We consider the energy range that probes the excitation of interband transitions, i.e., about 1–6 eV, and hence connect the experimental observation directly with the atomic structure and microscopic electronic response. Based on our results we confirm that the clean Si(100) surface is composed of a mixture of $c(4\times2)$ and $p(2\times2)$ reconstructions, with no $p(2\times1)$ present, and provide a detailed analysis of the energy loss peaks observed in the experiment.

II. THEORY

A. Theoretical model of REELS

We use a semiclassical dipole scattering theory that accounts for the long-range interaction between the incident electrons and the medium under study.[21,29] This theory assumes that the electron does not penetrate the crystal, and hence all losses occur in the vacuum. Assuming planar scattering and taking yz as being the scattering plane (z is the surface normal), the scattering probability is defined by

$$P(\mathbf{k},\mathbf{k}') = A(\mathbf{k},\mathbf{k}')\mathrm{Im}\ g(\mathbf{q}_\parallel,\omega), \tag{1}$$

where $\mathbf{k}$ and $\mathbf{k}'$ are the incident and scattered wave vectors. The kinematic factor, $A(\mathbf{k},\mathbf{k}')$,

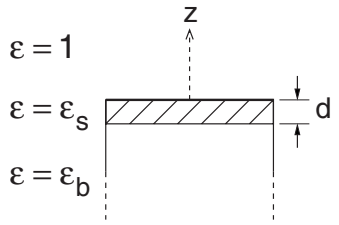

FIG. 2. Schematic representation of the constituent parts of the three-layer model of the surface.

$$A(\mathbf{k},\mathbf{k}') = \frac{2}{(ea_0\pi)^2}\frac{1}{\cos\ \theta_0}\frac{|\mathbf{k}'|}{|\mathbf{k}|}\frac{q_\parallel}{|q_\parallel^2+q_\perp^2|^2} \tag{2}$$

mostly describes the scattering geometry. The angle θ_0 is the direction of the incident beam with respect to the normal to the surface plane, and $\mathbf{q}_\parallel, q_\perp$ are the parallel and perpendicular components of the transferred momentum $\mathbf{q}=\mathbf{k}-\mathbf{k}'$. The loss function is defined by

$$\mathrm{Im}\ g(\mathbf{q}_\parallel,\omega) = \mathrm{Im}\frac{-2}{1+\varepsilon_{\mathrm{eff}}(\mathbf{q}_\parallel,\omega)} \tag{3}$$

and describes the dielectric response of the surface. If the surface was to be modeled as a semi-infinite truncated bulk, $\varepsilon_{\mathrm{eff}}$ would be replaced by ε_b and we would obtain the familiar expression of Ibach and Mills.[21]

In this work we adopt an anisotropic three-layer model of the surface as derived by Del Sole and co-workers.[30,31] The surface is modeled as in Fig. 2: a semi-infinite layer of vacuum; a surface layer of thickness d, represented by a surface dielectric *tensor* ε_s; and a semi-infinite bulk (dielectric function ε_b). The effective dielectric function is obtained as

$$\varepsilon_{\mathrm{eff}}(\mathbf{q}_\parallel,\omega) = \varepsilon_s\frac{\varepsilon_s+\varepsilon_b+(\varepsilon_b-\varepsilon_s)e^{-2q_\parallel\varepsilon_{\mathrm{aux}}d}}{\varepsilon_s+\varepsilon_b-(\varepsilon_b-\varepsilon_s)e^{-2q_\parallel\varepsilon_{\mathrm{aux}}d}}, \tag{4}$$

where ε_s and the auxiliary function $\varepsilon_{\mathrm{aux}}$ are functions of the y,z components of the dielectric tensor: $\varepsilon_s=\sqrt{\varepsilon_{s,y}(\omega)\varepsilon_{s,z}(\omega)}$ and $\varepsilon_{\mathrm{aux}}=\sqrt{\varepsilon_{s,y}(\omega)/\varepsilon_{s,z}(\omega)}$. This expression is equivalent to the more complicated expression given in Ref. 30.

Although the dielectric functions appearing in Eq. (4) are fully dependent on $q_\parallel$ and ω, such quantities are not easy to calculate since $\mathbf{q}$ and ω are not independent. Hence we make the approximation of replacing $\varepsilon_s(\mathbf{q},\omega)$ with the optical dielectric function $\varepsilon_s(\omega)\approx\lim_{\mathbf{q}\to0}\varepsilon_s(\mathbf{q},\omega)$. This appears to be a reasonable assumption since for most of the experiments modeled in this work, q is rather small.

B. First-principles scheme

We use density-functional theory in the local density approximation (DFT-LDA) within a plane-wave and pseudopotential framework. The ABINIT (Refs. 32 and 33) and PWSCF (Ref. 34) codes were used for computing the relaxed atomic structures, electronic band structures, and Kohn-Sham eigenvalues and eigenvectors required for the optical properties. However, since we found only minor differences between spectra computed with the two codes, we report for consis-

tency only the final spectra obtained using PWSCF. Standard norm-conserving pseudopotentials of the Hamann type[35] generated with the FHI98PP package[36] within the DFT-LDA (Perdew-Zunger parametrization[37]) framework were used along with a 30 Ry kinetic energy cutoff.

1. Geometric structure

A standard repeated-slab and supercell approach was adopted in order to model the surface structure. We use relatively thick slabs (16 atomic layers) separated by eight layers of vacuum (about 10 Å). We used the theoretical lattice constant, as determined at 30 Ry, of 5.393 Å. During the geometry optimization, the central four layers were fixed at the bulk positions and structures were relaxed until the Cartesian force components were less than 20 meV/Å. Our obtained structural parameters are similar to those obtained previously for this surface,[31] such as a dimer buckling of 0.755 Å and a dimer length of 2.33 Å.

2. Computation of energy loss and RA spectra

Optical and energy loss spectra were calculated using the YAMBO code.[38] We carried out careful convergence tests on the optical and energy loss properties with respect to the numbers of bands and **k** points. For the most converged calculations, we used dense **k**-point meshes for the three reconstructions, equivalent to 1152, 1024, and 800 points in the (1×1) Brillouin zone for the $c(4\times2)$, $p(2\times2)$, and $p(2\times1)$ structures, respectively.

3. Treatment of many-body effects

Spectra reported in this work, and the subsequent analysis, were carried out within the approximation of noninteracting particles [random-phase approximation (RPA)] using the DFT-LDA eigenvalues and wave functions. A straightforward scheme for incorporating many-body effects is to apply a "scissors" operator to the unoccupied states, following the recipe of Del Sole and Girlanda.[39] In this way we compensate for the well-known underestimation of the DFT-LDA band gap and partially account for self-energy and excitonic shifts in energy. A scissors shift of +0.5 eV has previously been determined in other works[40] on Si(100) as giving the best agreement with the experimental RA spectra. We also confirm this result from a comparison to the experimental RA data (see Fig. 5).

Nevertheless, this value may not consistently describe the energetic positions of all surface state features, which generally undergo many-body corrections different from bulk ones. In order to determine a more meaningful correspondence between surface-related experimental and theoretical energy loss peaks, we also performed some preliminary calculations including many-body effects on a smaller (12 layers) $c(4\times2)$ slab relaxed at a lower kinetic energy cutoff (12 Ry). These calculations, which are discussed in more detail in the Appendix, reveal that the EEL spectral line shape for this surface remains very similar when many-body effects are included. Therefore, allowing for the small energetic differences observed, it is reasonable to use the shifted RPA spectra to describe the experimental REELS data from now on.

III. TECHNICALITIES IN THE COMPUTATION OF REELS

A. Surface layer response

Equation (4) contains a single parameter d, corresponding to the thickness of the surface layer. Within the description of the three-layer model, an electron impinging on the surface feels the potential from this surface layer through its dielectric function ε_s as well as the potential of the bulk region. However, microscopic calculations generally output the dielectric function of the supercell ε_c. In previous works,[42] ε_s was extracted from ε_c by using the expression for a symmetric slab,

$$d_c\varepsilon_c(\omega) = d_b\varepsilon_b(\omega) + 2d\varepsilon_s(\omega), \tag{5}$$

where d_c and d_b are the thicknesses of the supercell and bulk region of the slab, respectively. Nevertheless, the *bulk* region of the slab may be not uniquely defined and this approach cannot always guarantee perfect cancellation of the bulklike layers in the supercell and may even lead to unphysical negative loss features.

A more reliable approach is to extract ε_s directly by projecting out the response of a defined surface layer using a *cutoff* function[43] in real space. For all experiments modeled, we confirmed that varying d by an atomic layer did not change the results very much. The dependence of the REEL spectra on the parameter d is illustrated in Fig. 3 for a typical spectrum and compared with the result obtained using Eq. (5). Clear differences are seen for small values of d, while the two methods become equivalent for $d>4$ layers.

B. Finite acceptance effects

In experimental EEL spectroscopy a detector with a finite aperture, typically about $1°-2°$, collects the scattered electrons (throughout this paper we have assumed an analyzer half-aperture angle of $\theta_{\text{det}}=1°$). To compute reliable quantitative spectra one should perform a numerical integration of the scattering cross section over the detector window. We achieve this by means of a Monte Carlo integration (random sampling) in the computation of the following integral over the circular detector:

$$\int A(\mathbf{k},\mathbf{k}')\text{Im}\, g(\mathbf{q}_\parallel,\omega)d\Omega. \tag{6}$$

In Fig. 4 we illustrate the importance of such numerical sampling by comparing a typical EEL spectrum calculated in this way (evaluated over ~1000 points) with spectra calculated taking a single random $\mathbf{q}_\parallel$ and by evaluating the mean value of the integrand. Although the peak positions are consistent, depending on the kinematic conditions, a large difference is found in the relative intensity of the peaks. In particular, taking an average value underestimates the contribution of small angle scattering which is enhanced at low energy by the kinematic factor $A(\mathbf{k},\mathbf{k}')$.

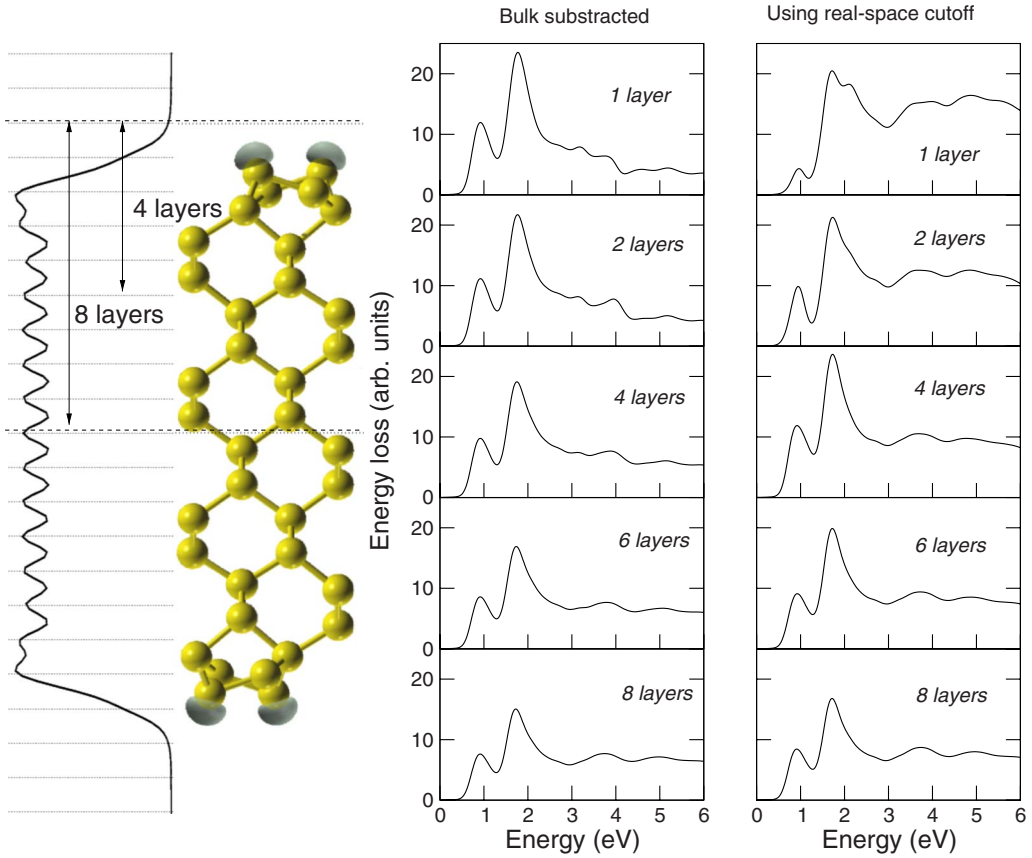

FIG. 3. (Color online) Left: schematic diagram of the Si(100)-$c(4\times2)$ slab and calculated layer averaged charge density; atomic layers are marked with horizontal lines. Right: dependence of a typical REEL spectrum on the value of surface layer thickness d using the two methods explained in the text. A mean value detector sampling approach has been used here (see Sec. III B).

C. Broadening

Inspection of Eq. (2) reveals that the cross section goes as $1/q^3$ as $\omega\to0$. Hence any features appearing in the loss function Im $g(\mathbf{q}_\parallel,\omega)$ at low energy are dramatically enhanced by $A(\mathbf{k},\mathbf{k}')$. From a computational point of view this means that unphysical features may appear close to the origin if a Lorentzian broadening is used when calculating the surface dielectric function of a system with a small band gap. We adopt, therefore, a tiny Lorentzian broadening of $\delta_L=0.006$ eV when calculating the dielectric functions and afterward convolute the loss spectra with a Gaussian function having full width at half maximum $\delta_G\sim0.3$ eV (where $\delta_G=2\sqrt{2\ln2}\sigma$, σ being the standard deviation) in order to approach the experimental resolution. These broadening factors have been used in all spectra reported in this work unless indicated otherwise.

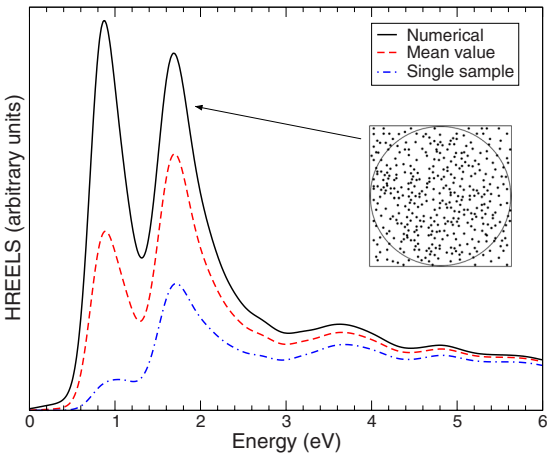

FIG. 4. (Color online) Dependence of typical REEL spectra on detector integration method: numerical Monte Carlo, mean value scheme, and single point sampling. Example shown for $c(4\times2)$ surface, averaged $\mathbf{q}_\parallel$; $E_0=40$ eV; $\theta_0=60°$; and $\theta_{\rm det}=1°$.

IV. RESULTS

A. Reflection anisotropy spectra

Several theoretical studies of optical spectra, namely, RA spectra, for the Si(100) surface have previously been carried out, including tight binding calculations,[44] discrete-dipole models,[45,46] *ab initio* calculations at the independent particle level,[18–20,40,47–49] as well as more recent studies including many-body effects.[50] As previously mentioned, it was found that the best agreement with the experimental RA data[41] is obtained when the $c(4\times2)$ or $p(2\times2)$ models are used in the calculations, while the $p(2\times1)$ gives poor agreement. Since we will use the same optical dielectric functions when computing the energy loss spectra, we show for complete-

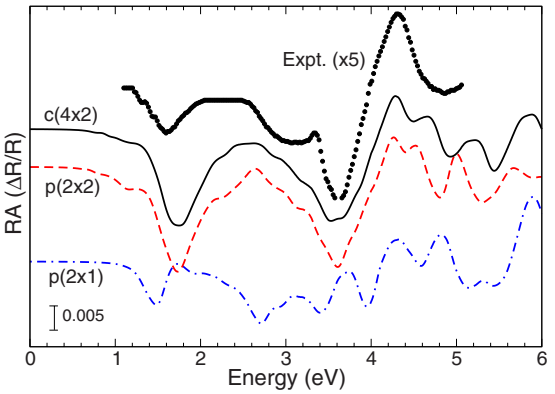

FIG. 5. (Color online) RA spectra of the $c(4\times2)$, $p(2\times2)$, and $p(2\times1)$ reconstructions of clean Si(100), compared with the experimental spectrum of the nominal surface (scaled by a factor of 5). Experimental data are taken from Ref. 41.

ness (in Fig. 5) the results of our own supercell calculations for the $c(4\times2)$, $p(2\times2)$, and $p(2\times1)$ reconstructions at the independent particle level. The reflectance anistropy is defined as

$$\mathrm{RA} = \frac{\Delta R_x}{R} - \frac{\Delta R_y}{R}, \tag{7}$$

where $\Delta R_i/R$ $(i=x,y)$ is the normalized reflectivity (i.e., relative to the Fresnel reflectivity). Throughout this work we will refer to the $[01\bar{1}]$ direction as x and the $[011]$ direction as y, with $[100]$ being the surface normal z. As expected, we find that both $c(4\times2)$ and $p(2\times2)$ spectra yield good agreement with the experimental data. The $p(2\times1)$ reproduces the low energy peak at 1.5 eV rather well, but the comparison worsens at higher energy. Unfortunately, no experimental data are available for the RA of Si(100) in the near-IR range, and hence information is limited to >1.1 eV. The good agreement with experiment provides an *a posteriori* justification for the scissors shift of +0.5 eV assumed in this work.

B. HREEL spectra at $E_0=40$ eV

We now consider the HREELS experiment of Farrell *et al.*[27] performed with a primary energy of $E_0=40$ eV. The loss spectrum roughly covers the same spectral range as the available RA data. At low energy, there is a one-to-one correspondence between RA spectroscopy and HREELS, as previously noted by Arciprete *et al.*[51] for the case of GaAs(001)-$c(4\times4)$. The experimental data, which are reproduced in Fig. 6, are characterized at low energy by two main features: a shoulder at 0.9 eV (S_0) and a broad peak around 1.4–2.0 eV (S_1), the latter which was reported to derive from surface states. The S_1 peak had been identified in early REELS studies (under different kinematic conditions) by Ibach and Rowe[22,25] at 1.7 ± 0.5 eV and by Maruno *et al.*[23] at about 2.0 eV. Other features appearing at about 3.5 and 5 eV have previously been identified in second-derivative spectra by Rowe and Ibach[22] at $E_0=100$ eV and are understood to derive from the bulk critical points, E_1 and E_2. In the experimental spectrum shown in Fig. 6 we have

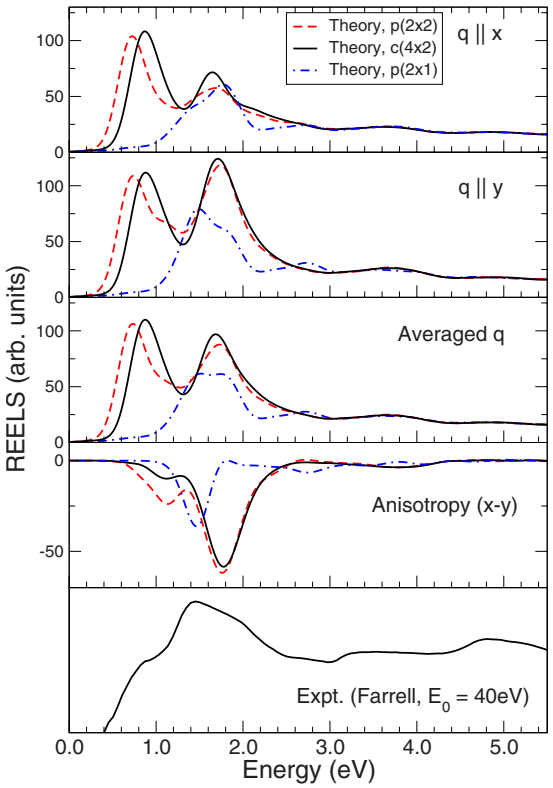

FIG. 6. (Color online) REEL spectra of $c(4\times2)$, $p(2\times2)$, and $p(2\times1)$ reconstructions of clean Si(100), and comparison with experiment (see Ref. 27): $E_0=40$ eV; $\theta_0=60°$. The surface thickness is assumed to be $d=8$ layers (plus one vacuum as shown in Fig. 3), i.e., the half slab. A background signal has been subtracted from the experimental spectrum (see text).

subtracted a background signal, taken to be that of the monohydride Si(100):H surface, also reported in Ref. 27.

The results of our first-principles calculations of HREELS are shown in Fig. 6 for the $p(2\times1)$, $p(2\times2)$, and $c(4\times2)$ reconstructions of Si(100). We report the REELS signal computed explicitly for transferred momenta $\mathbf{q}$ aligned parallel and perpendicular to the dimer rows, as well as the average value and the difference $x-y$. Due to the likelihood of different domains being present on the surface, the experimental spectra should be compared with the average value. The difference spectrum, or anisotropy, can be compared with the RA spectra of Fig. 5: indeed, the negative peak appearing at 1.6–1.8 eV corresponds well with the low energy peak in the RA.

From the comparison with the experimental HREELS data it is clear that the $p(2\times1)$ alone cannot reproduce the experimental signal since the shoulder at 0.8 eV (S_0) is missing from its theoretical spectrum. A similar observation was made by Gavioli *et al.*[28] based on tight binding calculations of the HREEL spectrum. As in the case of the RA, it is difficult to distinguish between the $c(4\times2)$ and $p(2\times2)$ calculated spectra. The S_0 peak appears at a slightly lower energy (by 0.1 eV) in the $p(2\times2)$ calculation; however, considering the approximations used (scissors shift), it is not sufficient to allow us to prefer the $c(4\times2)$ reconstruction over the $p(2\times2)$ based on these data alone.

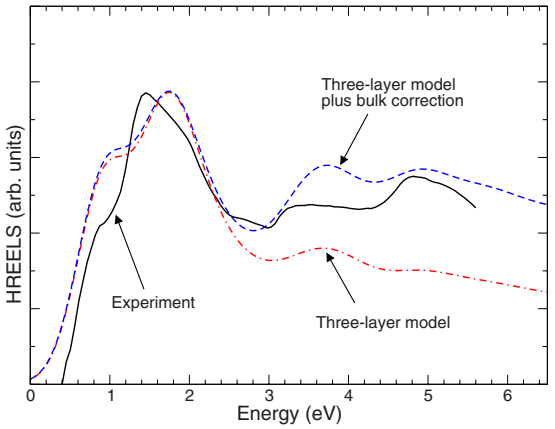

FIG. 7. (Color online) REEL spectra of Si(100)-$c(4\times2)$ calculated using a mixture of long-range reflection and short-range transmission loss functions [Eq. (8)], compared with experiment (see Ref. 27): E_0=40 eV; θ_0=60°.

As noted in Sec. II A, the three-layer model accounts only for losses occurring from scattering off long-range potentials (dipole scattering) above the surface. In reality, electrons with a 40 eV kinetic energy penetrate the surface by several atomic layers before elastic scattering occurs. As a result, features in the loss which arise from short-range scattering within the crystal itself (as occurs naturally in transmission EELS) are missing from our theory. Hence the calculated line shape differs significantly from the experimental one above 2.5 eV.

To counteract this deficiency of the theory, we augment the reflection loss term $g(\mathbf{q},\omega)$ with a second term that represents the transmission loss or bulk loss within the subsurface layers,

$$g'(\mathbf{q},\omega) = g(\mathbf{q},\omega) + K(\omega)\left\{\frac{-1}{\varepsilon_b}\right\}. \tag{8}$$

We define K in terms of the electronic penetration depth l as follows:

$$K(\omega) = \frac{l + \dfrac{1}{q_\parallel(\omega)}}{\dfrac{1}{q_\parallel(\omega)}} = 1 + q_\parallel(\omega)l, \tag{9}$$

where $1/q_\parallel$ is the estimated extension of the electric field inside the sample. Since l cannot be easily calculated, we have estimated it from the universal electron scattering curve as being ~6 Å for a kinetic energy of 40 eV. The result of including this extra corrective term [using Eq. (8)] is shown in Fig. 7. In order to mimic the low energy part of the experiment, we have used a larger broadening (δ_G=0.7 eV) and detector aperture ($\theta_{\rm det}$=2°) than those used previously (δ_G=0.3 eV, $\theta_{\rm det}$=1°). The three-layer model already accounts well for losses within the surface layer, and the extra term improves the agreement near the critical point energies. Such an augmented loss technique may be useful for providing a more complete model of EELS in nanostructures, for instance, where the weights of surface and bulk losses can be relatively similar.

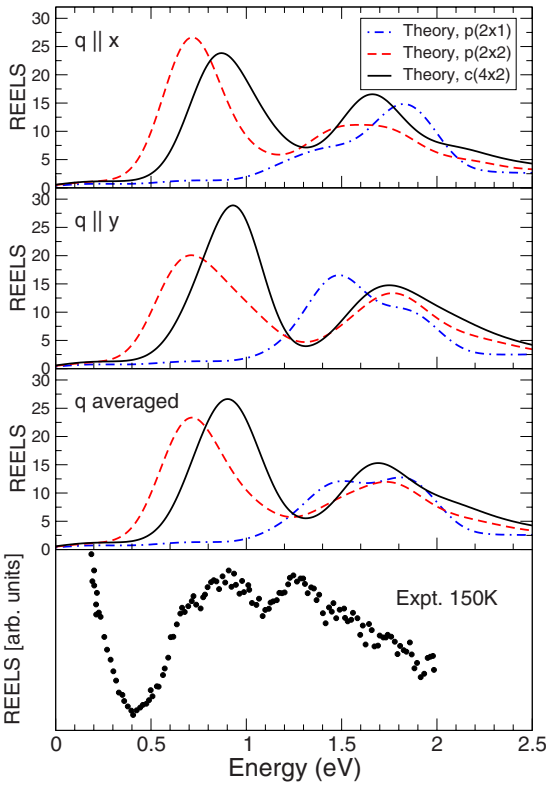

FIG. 8. (Color online) REEL spectra of $p(2\times1)$, $p(2\times2)$, and $c(4\times2)$ reconstructions of clean Si(100) for low energy incident beam (E_0=7 eV; θ_0=60°). Surface thickness d=2 atomic layers.

C. Low-energy REEL spectra

In the remaining sections of this paper, we consider data only up to 2.5 eV and can henceforth safely neglect the additional term in Eq. (8), i.e., we consider only the loss terms due to reflection. We reproduce in the bottom panel of Fig. 8 the HREEL data for low energy incident electrons reported by Gavioli *et al.*[28] (E_0~7 eV; θ_0~60°) at 150 K. In addition to the previously mentioned S_0 and S_1 peaks (the latter now appearing at 1.15–1.35 eV), the high resolution spectra succeed in resolving a further shoulder at 0.68 eV. Results of our *ab initio* simulation of this HREELS experiment are also reported in the figure. As noted for the E_0=40 eV data, it is clear that the $p(2\times1)$ model does not yield the correct line shape, as the S_0 peak is missing for this structure. Both $c(4\times2)$ and $p(2\times2)$ structures succeed in reproducing the double-peaked structure observed in the experiments. The S_0 peak at 0.9 eV is well reproduced by the $c(4\times2)$ model, while the shoulder observed at 0.68 eV points to the coexistence of $p(2\times2)$ on the predominantly $c(4\times2)$ surface (total energy calculations find that their energy of formation is almost equal). As discussed in Sec. II B, the calculated energetic position of the S_1 peak is overestimated when adopting a scissors shift of 0.5 eV.

D. Analysis of S_0 and S_1

We now interpret the experimental peaks observed in the high resolution REEL spectra at low energy ($E_0\approx7$ eV).

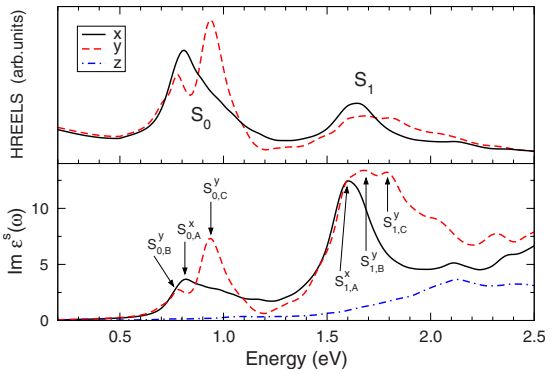

FIG. 9. (Color online) HREELS along x and y (top) and surface dielectric functions (along x, y, and z directions) for E_0=7 eV, θ_0 =60°; a scissor shift of +0.5 eV is applied.

Figure 9 compares the calculated surface dielectric function ε_s with the $c(4\times2)$ HREEL spectra, calculated using a lower broadening to enhance the spectral features. From the one-to-one correspondence between the upper and lower panels it is clear that the S_0 and S_1 peaks can be understood by analyzing the various peaks in Im ε_s [see Eq. (A1)], which can easily be achieved by analyzing the oscillator strength $|P_{v,c,\mathbf{k}}|^2$.

In Fig. 10 we show the total oscillator strength $\bar{P}_E(\mathbf{k})$ for each peak as a function of $\mathbf{k}$ within the $c(4\times2)$ surface Brillouin zone. The function $\bar{P}_E(\mathbf{k})$ is a measure of the total transition strength within an energy window of width 2δ =0.1 eV centered on the chosen peak energy E,

$$\bar{P}_E(\mathbf{k}) = \sum_{v,c} |P_{v,c,\mathbf{k}}|^2 \quad \text{for } E-\delta < E_{c\mathbf{k}} - E_{v\mathbf{k}} < E+\delta. \tag{10}$$

From Fig. 10 it is clear that S_0 arises from transitions located around the Γ point for both polarizations, while S_1 arises

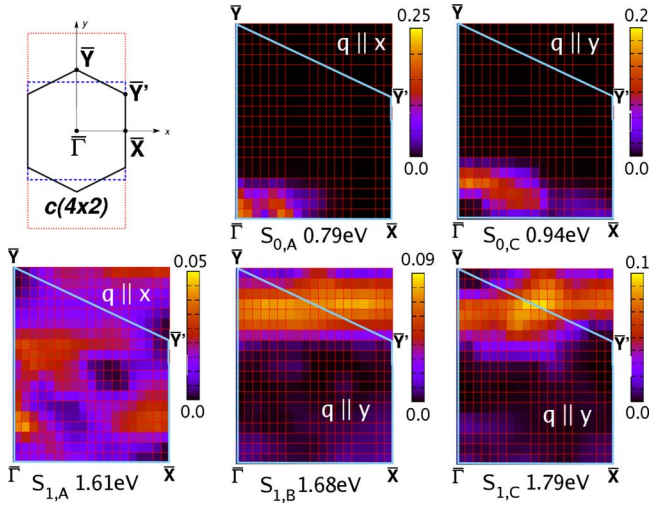

FIG. 10. (Color online) Total oscillator strength $\bar{P}_E(\mathbf{k})$ (in Hartree) corresponding to the S_0 and S_1 HREELS peaks as a function of $\mathbf{k}$ within the irreducible part of the $c(4\times2)$ Brillouin zone. $\bar{P}_E(\mathbf{k})$ is shown explicitly for the components $S_{0,A}$, $S_{1,A}$, etc., indicated in Fig. 9. The polarization of the transition is indicated in each case.

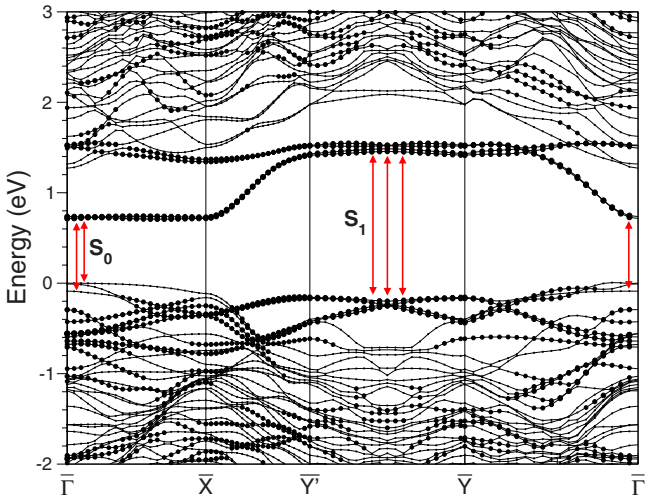

FIG. 11. (Color online) Band structure of the $c(4\times2)$ surface: surface localized states are indicated by the heavier dots. A rigid scissor shift of +0.5 eV has been applied to unoccupied bands.

mostly for $\mathbf{q}\|y$ from transitions along the $\bar{Y}-\bar{Y}'$ BZ edge. The latter finding invalidates the deductions made in the work of Farrell *et al.*[27]

The location of these transitions with respect to the surface band structure is shown in Fig. 11. Our band structure calculation for the clean $c(4\times2)$ surface compares well with that previously published by Fuchs.[20] Furthermore, we show in Fig. 12 a plot of $|\psi_{n,\mathbf{k}}|^2$ for the valence and conduction band states taking part in the strongest transitions. Hence a complete analysis of the HREELS spectra is obtained from Figs. 9–11. The S_0 peak is due to transitions between bulk states at the valence band maximum (at Γ) and unoccupied surface states lying within the fundamental bulk band gap about 0.8 eV higher (indicated in Fig. 11). We have explained the origin of the S_0 peak as observed by Farrell. This peak also corresponds to the feature observed below 1 eV in SDR studies by Chabal *et al.*[53] Transitions occur symmetrically around Γ, explaining why the anisotropy of the response is low (Fig. 6). We confirm that the S_1 structure derives from transitions between π and π^* orbitals, as previously determined from theoretical studies of the optical properties.[18,43,48]

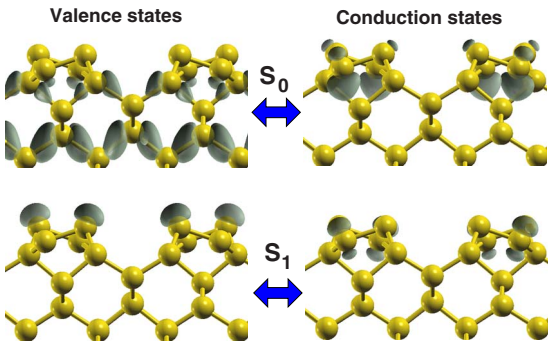

FIG. 12. (Color online) Isosurface plots of $|\psi_{n\mathbf{k}}(r)|^2$ for representative states involved in transitions giving rise to the S_0 (top) and S_1 (bottom) HREELS peaks. Plots were obtained using the XCRYSDEN (Ref. 52) package.

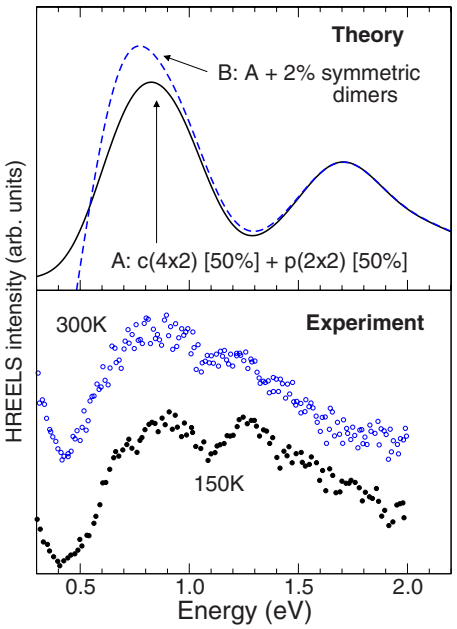

FIG. 13. (Color online) Top: computed HREELS spectra for a 1:1 mixture of the $c(4\times2)$ and $p(2\times2)$ reconstructions (a), along with the same spectrum containing a 2% average fraction of the symmetric dimer $p(2\times1)$ spectrum (b). Bottom: temperature dependent experimental data of Gavioli *et al.* (Ref. 28), stacked vertically for clarity. Kinematic parameters: $E_0=7$ eV; $\theta_0=60°$; surface thickness $d=2$ atomic layers.

E. Discussion

Having thoroughly analyzed the primary HREELS peaks, we can now discuss the behavior of the HREELS spectra as a function of temperature and hence make some conclusions about the structure of the Si(100) surface. Gavioli *et al.*[28] presented spectra obtained below (150 K) and above (300 K) the well-known order-disorder transition temperature occurring at about 200 K. The two spectra are reproduced in the bottom panel of Fig. 13. From LEED experiments it is known that in the low T regime the Si(100) surface exhibits a $c(4\times2)$ periodicity; a $p(2\times1)$ pattern occurs above the transition temperature. With increasing T, the intensity of the S_0 peak was reported to increase relative to the S_1 peak and the shoulder at 0.68 eV was shown to almost disappear. Although thermal broadening gives rise to an overall reduction in intensity with increasing temperature, it should influence all the peaks equally and hence cannot explain the line shape change at 300 K.

Our calculated REELS spectra indicate that the 150 K data can be thoroughly explained with a mixture of $c(4\times2)$ and $p(2\times2)$ structures, with the former responsible for the main peak at 0.9 eV and the latter giving rise to the 0.68 eV shoulder (see Fig. 8). Regarding the 300 K data, if we only consider the three reconstruction models of Fig. 1, it is clear that the relative reduction in S_1 can only be explained by a reduction in the amount of $p(2\times1)$ on the surface, as this structure only contributes to S_1. However, this would imply that $p(2\times1)$ structures are present at 150 K, which does not agree with the STM observations of an ordered $c(4\times2)$ surface.[2] One might anyway expect the amount of $p(2\times1)$ to *increase* above the order-disorder transition temperature.

To explain the temperature dependence of the spectra, we find it necessary to infer the presence of a small amount of *symmetric* dimers, as was also assumed in Ref. 28. Being a very fast process, REELS makes an instantaneous snapshot of the surface structure during the dimer flipping occurring dynamically at 300 K. Although the dimers remain asymmetric for the longest time period [whether in the $c(4\times2)$ or $p(2\times2)$ phase], a small amount of symmetric dimer structure will be probed by the impinging electrons. By performing a further REELS calculation for the symmetric dimer structure [in a $p(2\times1)$ cell], we have determined that the addition of only a small fraction (2%) of this reconstruction is required to recover the observed relative peak intensity between S_0 and S_1, as shown in Fig. 13. This fraction is less than the 5% assumed in Ref. 28 since in that work the spectrum of clean $c(4\times2)$ was not considered as a basis for the low temperature spectrum.

V. CONCLUSIONS

We have presented a theoretical study of the electron energy loss of the Si(100) surface. Reconstructions of $p(2\times1)$, $p(2\times2)$, and $c(4\times2)$ symmetries were considered. Calculations of reflectance anisotropy spectra are in agreement with previous works. REEL spectra were calculated for two experimental setups according to the available experimental data. We confirmed that $p(2\times1)$ cannot be the predominant reconstruction present on the actual surface at 150 or 300 K, and we find evidence that the low temperature surface is a mixture of $c(4\times2)$ and $p(2\times2)$ reconstructions.

The origin of the low energy S_0 and S_1 peaks occurring in experimental HREELS spectra has been carefully analyzed for the $c(4\times2)$ model. The former peak arises from transitions involving bulk states around Γ and surface states below the band gap and is due to the surface band folding of $c(4\times2)$ and $p(2\times2)$. S_1, instead, involves only surface states. The temperature dependence of the observed spectra has been explained by assuming that a small amount of symmetric dimers, present above the order-disorder transition at 200 K, are instantaneously probed during the REELS experiment. The low temperature spectrum can be completely explained by means of a mixture of $c(4\times2)$ (primarily) and $p(2\times2)$ structures. This work constitutes a starting point from which to analyze the experimental energy loss spectra of oxidized silicon surfaces.

ACKNOWLEDGMENTS

This work was supported by the EU through the Nanoquanta Network of Excellence (Grant No. NMP4-CT-2004-500198) and the ETSF–I3 (Grant No. 211956). We thank L. Gavioli and M. Palummo for useful discussions and acknowledge generous supercomputing support from CINECA (account cne0fm2h) and CASPUR.

APPENDIX: MANY-BODY EFFECTS

In this appendix we estimate the influence of many-body effects on the EEL spectrum of Si(100)-$c(4\times2)$ by means of

first-principles calculations using the YAMBO (Ref. 38) code. Self-energy corrections were computed (within the so-called *GW* approximation), while excitonic and local field effects were accounted for by means of solving the Bethe-Salpeter equation (BSE).[54] In the *GW* part of the calculation, we calculated the screening matrix $\varepsilon^{-1}_{\mathbf{G},\mathbf{G}'}(\mathbf{q},\omega)$ using a plasmon pole model, including 765 G vectors to construct the matrix and 21 $\mathbf{q}$ points in the irreducible part of the Brillouin zone. The correlation part of the self-energy (Σ_c) was calculated using 765 plane waves and 750 bands, while 4021 plane waves were used in computing the exchange part (Σ_x). The Bethe-Salpeter equation was solved using the Haydock recursion method.[55,56] Since we focus here on the low energy part of the spectrum ($E<3$ eV), we found it sufficient to include only 30 valence and 30 conduction bands to describe the imaginary part of the dielectric function. Further details of the approach are beyond the scope of this paper but can be found, for instance, in other publications by some of us.[31]

Two sets of experimental HREELS data are available below 2.5 eV: Gavioli *et al.*,[28] taken at 150 K, and an earlier work by Farrell *et al.*[27] Their spectra are reproduced in Fig. 14, and both show the so-called S_0 and S_1 peaks. Although the kinematic setup is very similar in both cases, it is notable that the two spectra disagree in the energetic position of the S_1 peak by as much as 0.4 eV.

We compare these spectra with calculations of the imaginary part of the supercell dielectric function obtained with (*GW*+BSE) and without (RPA+scissors) many-body effects. For $\mathbf{q}_\parallel d \gg 1$ and an isotropic ε_s, Eq. (3) reduces to

$$\mathrm{Im}\, g(\mathbf{q},\omega) \approx \mathrm{Im}\left[\frac{-2}{1+\varepsilon_s}\right] = \frac{\varepsilon_s''}{(1+\varepsilon_s')^2+(\varepsilon_s'')^2}, \quad \text{(A1)}$$

i.e., directly related to the imaginary part of ε_s. In our case, $\mathbf{q}_\parallel d \simeq 1$, and hence Eq. (A1) should give a rough estimate of the experimental HREELS peak positions. From Fig. 14 it is clear that the *GW*+BSE results give a better agreement with the data of Gavioli *et al.*,[28] while the RPA+scissors calculation gives a misleadingly good comparison with the S_1 peak of Farrell *et al.*[27] (note that a better spectral resolution was obtained in the work of Gavioli *et al.*[28]). It is important to note, however, that the spectral shapes are very similar. Hence, allowing for the discrepancy in energy, it is reasonable to use the RPA spectra to describe the experimental REELS data for this surface.

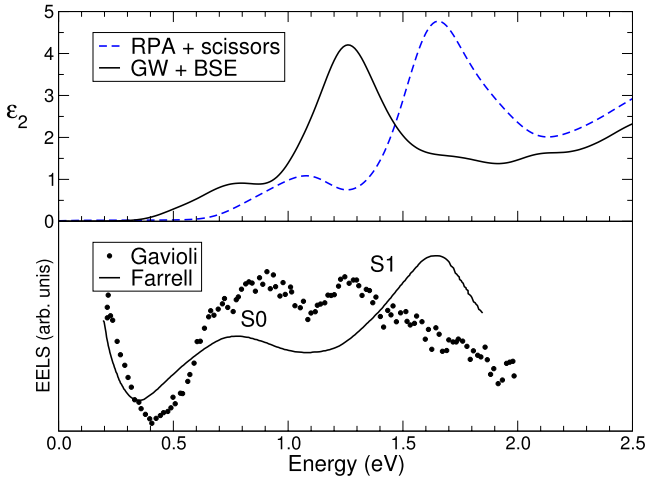

FIG. 14. (Color online) Top: computed ε_s (averaged over q) at the RPA+scissors and *GW*+BSE levels. Bottom: experimental data for similar experimental kinematic conditions, taken from Gavioli *et al.* (Ref. 28) and Farrell *et al.* (Ref. 27).

[1] R. Schlier and H. E. Farnsworth, J. Chem. Phys. **30**, 917 (1959).
[2] M. Ono, A. Kamoshida, N. Matsuura, E. Ishikawa, T. Eguchi, and Y. Hasegawa, Phys. Rev. B **67**, 201306(R) (2003).
[3] K. Sagisaka, D. Fujita, and G. Kido, Phys. Rev. Lett. **91**, 146103 (2003).
[4] J. Shoemaker, L. W. Burggraf, and M. S. Gordon, J. Chem. Phys. **112**, 2994 (2000).
[5] A. Ramstad, G. Brocks, and P. J. Kelly, Phys. Rev. B **51**, 14504 (1995).
[6] D. J. Chadi, Phys. Rev. Lett. **43**, 43 (1979).
[7] J. Ihm, D. H. Lee, J. D. Joannopoulos, and J. J. Xiong, Phys. Rev. Lett. **51**, 1872 (1983).
[8] T. Tabata, T. Aruga, and Y. Murata, Surf. Sci. **179**, L63 (1987).
[9] S. Yoshida, T. Kimura, O. Takeuchi, K. Hata, H. Oigawa, T. Nagamura, H. Sakama, and H. Shigekawa, Phys. Rev. B **70**, 235411 (2004).
[10] J. Nakamura and A. Natori, Phys. Rev. B **71**, 113303 (2005).
[11] K. Sagisaka and D. Fujita, Phys. Rev. B **71**, 245319 (2005).
[12] L. Kantorovich and C. Hobbs, Phys. Rev. B **73**, 245420 (2006).
[13] K. Seino, W. G. Schmidt, and F. Bechstedt, Phys. Rev. Lett. **93**, 036101 (2004).
[14] T. Shirasawa, S. Mizuno, and H. Tochihara, Phys. Rev. Lett. **94**, 195502 (2005).
[15] A. I. Shkrebtii, R. Di Felice, C. M. Bertoni, and R. Del Sole, Phys. Rev. B **51**, R11201 (1995).
[16] M. Kutschera, M. Weinelt, M. Rohlfing, and T. Fauster, Appl. Phys. A: Mater. Sci. Process. **88**, 519 (2007).
[17] M. Weinelt, M. Kutschera, R. Schmidt, C. Orth, T. Fauster, and M. Rohlfing, Appl. Phys. A: Mater. Sci. Process. **80**, 995 (2005).
[18] M. Palummo, G. Onida, R. Del Sole, and B. S. Mendoza, Phys. Rev. B **60**, 2522 (1999).
[19] F. Fuchs, W. G. Schmidt, and F. Bechstedt, Phys. Rev. B **72**, 075353 (2005).
[20] F. Fuchs, Master thesis, Friedrich-Schiller-Universität, Jena, Germany, 2004.
[21] H. Ibach and D. L. Mills, *Electron Energy Loss Spectroscopy and Surface Vibrations* (Academic, New York, 1982).
[22] J. E. Rowe and H. Ibach, Phys. Rev. Lett. **31**, 102 (1973).
[23] S. Maruno, H. Iwasaki, K. Horioka, S.-T. Li, and S. Nakamura, Phys. Rev. B **27**, 4110 (1983).
[24] H. Ibach and J. E. Rowe, Phys. Rev. B **10**, 710 (1974).

[25] H. Ibach and J. E. Rowe, Phys. Rev. B **9**, 1951 (1974).
[26] R. Ludeke and A. Koma, Phys. Rev. Lett. **34**, 1170 (1975).
[27] H. H. Farrell, F. Stucki, J. Anderson, D. J. Frankel, G. J. Lapeyre, and M. Levinson, Phys. Rev. B **30**, 721 (1984).
[28] L. Gavioli, M. Grazia Betti, C. Mariani, A. Shkrebtii, R. Del Sole, C. Cepek, A. Goldoni, and S. Modesti, Surf. Sci. **377-379**, 360 (1997).
[29] H. Lüth, *Surfaces and Interfaces of Solid Materials* (Springer, Berlin, 1995).
[30] A. Selloni and R. Del Sole, Surf. Sci. **168**, 35 (1986).
[31] M. Palummo, O. Pulci, A. Marini, L. Reining, and R. Del Sole, Phys. Rev. B **74**, 235431 (2006).
[32] X. Gonze *et al.*, Comput. Mater. Sci. **25**, 478 (2002).
[33] The ABINIT code is a common project of the Université Catholique de Louvain, Corning Incorporated, and other contributors (http://www.abinit.org).
[34] QUANTUM-ESPRESSO is a community project for high-quality quantum-simulation software based on density-functional theory and coordinated by Paolo Giannozzi (see http://www.quantum-espresso.org and http://www.pwscf.org).
[35] D. R. Hamann, Phys. Rev. B **40**, 2980 (1989).
[36] http://www.fhi-berlin.mpg.de/th/fhi98md/fhi98PP/
[37] J. P. Perdew and A. Zunger, Phys. Rev. B **23**, 5048 (1981).
[38] YAMBO is a code based on many-body perturbation theory for calculating excited states and is released under the GPL 2.0 license. See A. Marini, C. Hogan, D. Varsano, and M. Gruning, Comput. Phys. Commun. (to be published); http://www.yambo-code.org
[39] R. Del Sole and R. Girlanda, Phys. Rev. B **48**, 11789 (1993).
[40] A. Incze, R. Del Sole, and G. Onida, Phys. Rev. B **71**, 035350 (2005).
[41] R. Shioda and J. van der Weide, Phys. Rev. B **57**, R6823 (1998).
[42] R. Del Sole, W. L. Mochan, and R. G. Barrera, Phys. Rev. B **43**, 2136 (1991).
[43] C. Hogan, R. Del Sole, and G. Onida, Phys. Rev. B **68**, 035405 (2003).
[44] A. I. Shkrebtii and R. Del Sole, Phys. Rev. Lett. **70**, 2645 (1993).
[45] B. S. Mendoza, F. Nastos, N. Arzate, and J. E. Sipe, Phys. Rev. B **74**, 075318 (2006).
[46] C. D. Hogan and C. H. Patterson, Phys. Rev. B **57**, 14843 (1998).
[47] L. Kipp, D. K. Biegelsen, J. E. Northrup, L.-E. Swartz, and R. D. Bringans, Phys. Rev. Lett. **76**, 2810 (1996).
[48] C. Kress, A. I. Shkrebtii, and R. Del Sole, Surf. Sci. **377-379**, 398 (1997).
[49] V. I. Gavrilenko and F. H. Pollak, Phys. Rev. B **58**, 12964 (1998).
[50] M. Palummo, N. Witkowski, O. Pluchery, R. Del Sole, and Y. Borensztein, Phys. Rev. B **79**, 035327 (2009).
[51] F. Arciprete, C. Goletti, E. Placidi, P. Chiaradia, M. Fanfoni, F. Patella, C. Hogan, and A. Balzarotti, Phys. Rev. B **68**, 125328 (2003).
[52] A. Kokalj, Comput. Mater. Sci. **28**, 155 (2003) (http://www.xcrysden.org/).
[53] Y. J. Chabal, S. B. Christman, E. E. Chaban, and M. T. Yin, J. Vac. Sci. Technol. A **1**, 1241 (1983).
[54] S. Albrecht, L. Reining, R. Del Sole, and G. Onida, Phys. Rev. Lett. **80**, 4510 (1998).
[55] L. X. Benedict and E. L. Shirley, Phys. Rev. B **59**, 5441 (1999).
[56] R. Haydock, Comput. Phys. Commun. **20**, 11 (1980).